nature genetics

SUPPLEMENTARY INFORMATION

https://doi.org/10.1038/s41588-018-0155-3

In the format provided by the authors and unedited.

Genome-scale analysis identifies paralog lethality as a vulnerability of chromosome 1p loss in cancer

Srinivas R. Viswanathan[1,2,3], Marina F. Nogueira[1,2,12], Colin G. Buss[4,5,12], John M. Krill-Burger[2], Mathias J. Wawer[6], Edyta Malolepsza[2,7], Ashton C. Berger[1,2], Peter S. Choi[1,2,3], Juliann Shih[2], Alison M. Taylor[1,2,3], Benjamin Tanenbaum[2], Chandra Sekhar Pedamallu[1], Andrew D. Cherniack[2], Pablo Tamayo[2,8], Craig A. Strathdee[2], Kasper Lage[2,7], Steven A. Carr[2], Monica Schenone[2], Sangeeta N. Bhatia[2,3,4,5,9,10,11], Francisca Vazquez[2], Aviad Tsherniak[2], William C. Hahn[1,2,3] and Matthew Meyerson[1,2,3]*

[1]Department of Medical Oncology, Dana-Farber Cancer Institute, Boston, MA, USA. [2]Broad Institute of MIT and Harvard, Cambridge, MA, USA. [3]Harvard Medical School, Boston, MA, USA. [4]Harvard-MIT Department of Health Sciences and Technology, Institute for Medical Engineering and Science, Massachusetts Institute of Technology, Boston, MA, USA. [5]Koch Institute for Integrative Cancer Research, Massachusetts Institute of Technology, Cambridge, MA, USA. [6]Chemical Biology and Therapeutics Science Program, Broad Institute of Harvard and MIT, Cambridge, MA, USA. [7]Department of Surgery, Massachusetts General Hospital, Boston, MA, USA. [8]UCSD Moores Cancer Center and Department of Medicine, University of California, San Diego, La Jolla, CA, USA. [9]Howard Hughes Medical Institute, Chevy Chase, MD, USA. [10]Department of Electrical Engineering and Computer Science, Massachusetts Institute of Technology, Cambridge, MA, USA. [11]Department of Medicine, Brigham and Women's Hospital, Boston, MA, USA. [12]These authors contributed equally: Marina F. Nogueira, Colin G. Buss. *e-mail: matthew_meyerson@dfci.harvard.edu

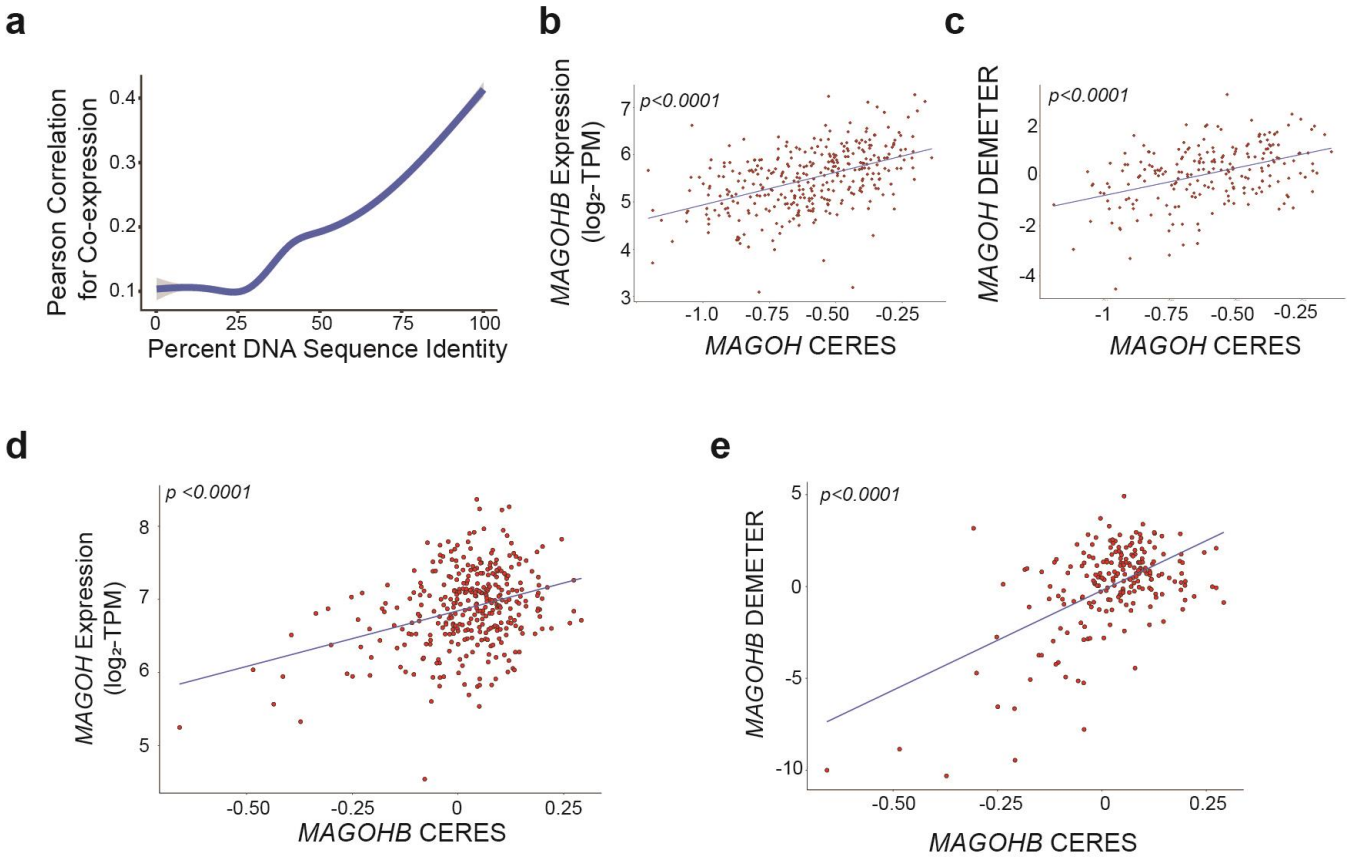

Supplementary Figure 1

Supplementary Figure 1

***MAGOH and MAGOHB* score as reciprocal paralog dependencies in both genome-scale CRISPR and shRNA screening datasets.**

a, Plot of the percentage DNA sequence identity between gene pairs versus Pearson correlation for their co-expression across the CCLE cell lines (n = 93,433 gene pairs plotted). The solid line shows the mean; the shaded region shows the standard error. **b**, Correlation between *MAOGHB* expression (y axis) and *MAGOH* dependency in CRISPR data (x axis). Pearson's r^2 = 0.2235 (n = 336 cell lines plotted). **c**, Correlation between *MAGOH* gene dependencies in shRNA (y axis) and CRISPR (x axis) data. Pearson's r^2 = 0.1763 (n = 215 cell lines plotted). **d**, Correlation between *MAGOH* expression (y axis) and *MAGOHB* dependency in CRISPR data (x axis). Pearson's r^2 = 0.1113 (n = 336 cell lines plotted). **e**, Correlation between *MAGOHB* gene dependencies in shRNA (y axis) and CRISPR (x axis) data. Pearson's r^2 = 0.3068 (n = 215 cell lines plotted).

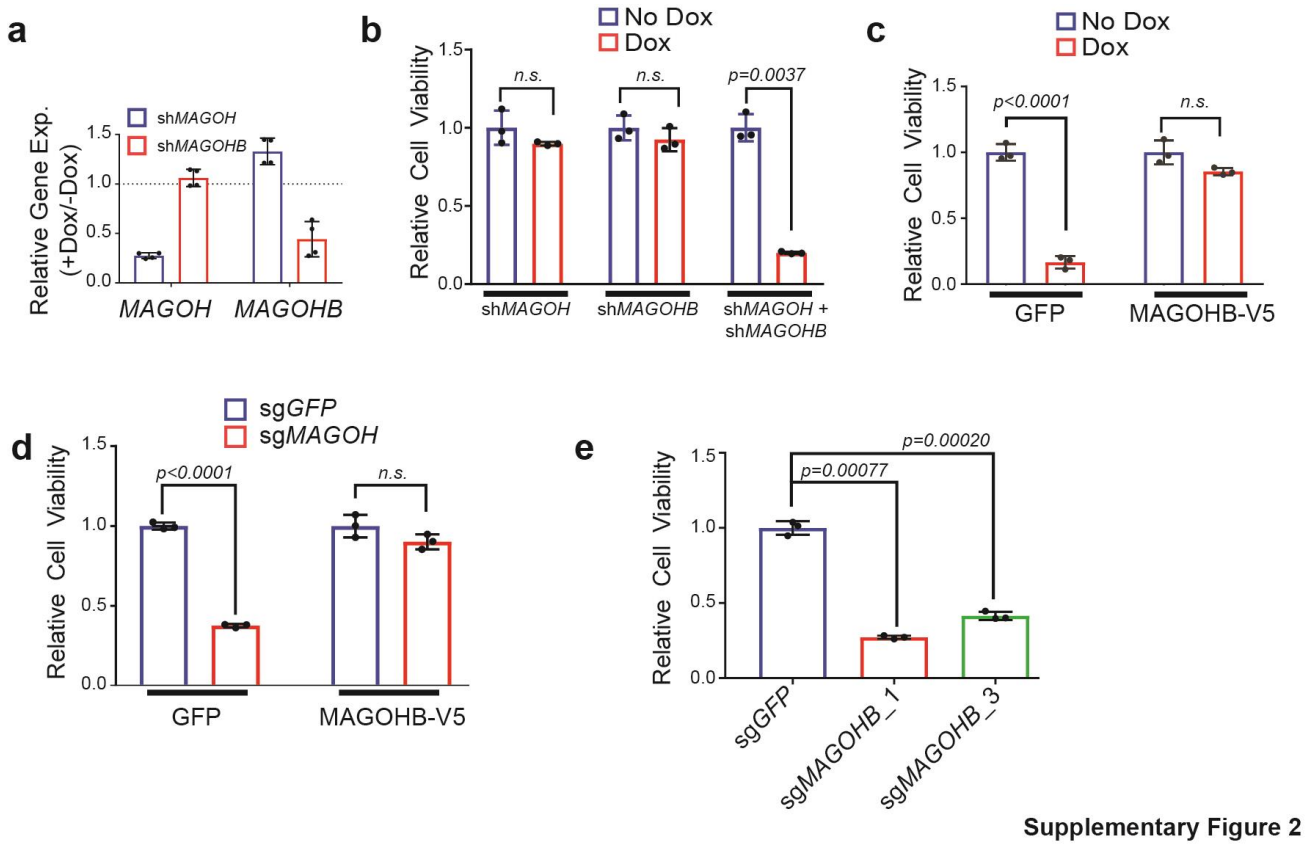

Supplementary Figure 2

Supplementary Figure 2

Validation of reciprocal *MAGOH*/*MAGOHB* dependencies.
a, Validation of selective *MAGOH* and *MAGOHB* knockdown using doxycycline-inducible shRNAs against *MAGOH* or *MAGOHB* in Heya8 cells. Expression levels of each paralog are shown relative to the no-knockdown (–Dox) condition in each case. Data are presented as mean ± s.d., *n* = 4 technical replicates. **b**, Cell viability was measured in Heya8 cells (which do not have deletions in either *MAGOH* or *MAGOHB*) upon knockdown of *MAGOH*, *MAGOHB*, or both. **c**, Cell viability measured upon *MAGOH* knockdown (using Dox-inducible shRNA) in hemizygous *MAGOHB*-deleted Huh1 cells with or without reconstitution of MAGOHB-V5. **d**, Cell viability measured upon *MAGOH* knockout (using sgRNA) in *MAGOHB*-deleted Huh1 cells with or without reconstitution of MAGOHB-V5. **e**, Validation of *MAGOHB* dependency in *MAGOH*-deleted H1437 cells using either control sgRNA (sgGFP) or two different sgRNAs against *MAGOHB*. For **b**–**e,** error bars show mean ± s.d., *n* = 3 replicates from a representative experiment repeated twice**;** *P* value by two-tailed, two-sample *t* test.

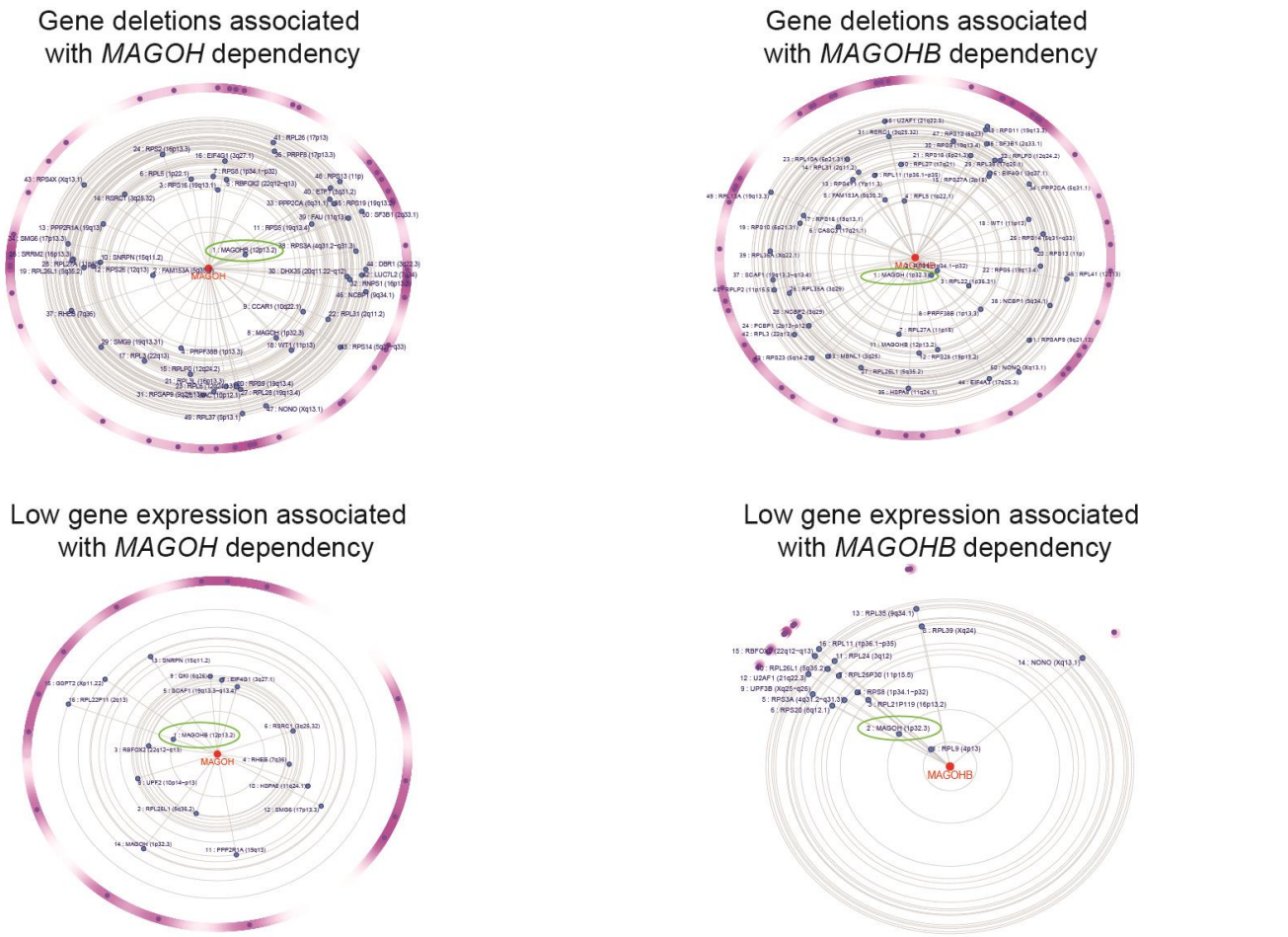

Supplementary Figure 3

Supplementary Figure 3

***MAGOH* and *MAGOHB* dependencies are associated with deletion/low expression of the partner paralog.**

Radial plots showing association of the top copy number alterations (top row) or gene expression changes (bottom row) correlated to *MAGOH* (left column) or *MAGOHB* (right column) dependency, among splicing and NMD-related genes. The radial plot depicts both the association of copy number/gene expression correlates with the target dependency profile (either *MAGOH* or *MAGOHB* dependency) and with each other. The radial distance of each feature (blue dot) from the dependency target (red) is inversely proportional to the information coefficient score between that feature and the target. The angular distances between features are based on the association matrix of information coefficient scores generated when comparing the top features with each other. If two features are close in angular distance, they have a higher information coefficient value with each other as compared to features that are father away in angular distance. *MAGOH*/*MAGOHB* dependencies are uniquely predicted by low expression or copy number loss of the partner paralog (circled in green).

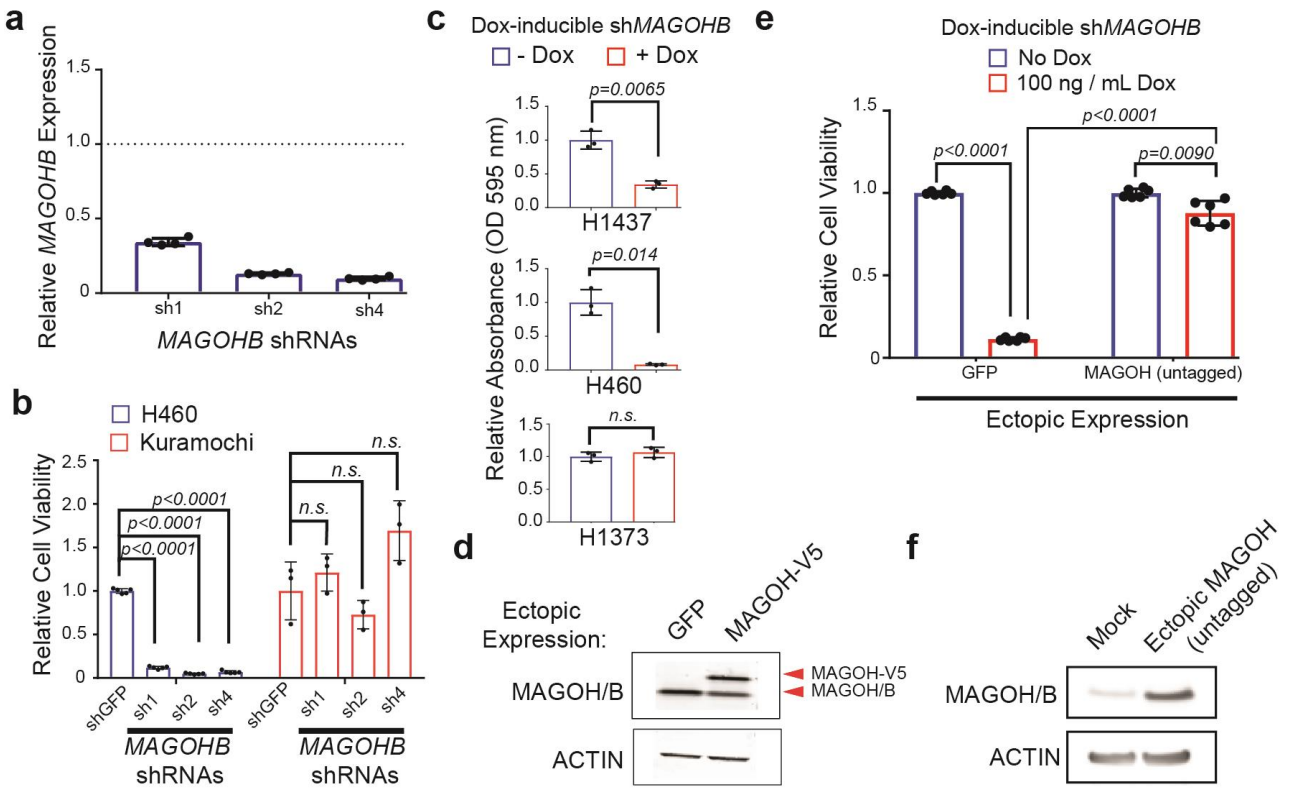

Supplementary Figure 4

Supplementary Figure 4

Additional validation of *MAGOHB* dependency in cells with hemizygous *MAGOH* loss.
a, Validation of *MAGOHB* knockdown with multiple *MAGOHB* shRNAs. H460 cells were transduced with lentivirus expressing either control shRNA (sh*GFP*) or shRNAs against *MAGOHB* in the pLKO.1 vector. *MAGOHB* knockdown was assessed 72 h after selection using quantitative PCR. Expression levels are shown as normalized to control (sh*GFP*) condition (dotted line). Data are presented as mean ± s.d., *n* = 4 technical replicates. **b**, Validation of selective *MAGOHB* dependency in *MAGOH*-deleted cells. Hemizygous *MAGOH*-deleted H460 cells or Kuramochi cells (no *MAGOH* deletion) were transduced with lentivirus encoding either control shRNA (shGFP) or shRNAs against *MAGOHB* in the pLKO.1 vector. Cell viability was assessed by CellTiterGlo 9 d after infection. Data are presented as mean ± s.d., *n* = 3 replicates (Kuramochi), *n* = 5 replicates (H460); *P* value by two-tailed two-sample *t* test. **c**, Quantification of colony formation assay (related to Fig. 1e). Following crystal violet staining, wells were destained and measurement of absorbance at 595 nm was performed for quantification of colony number. Data are presented as mean ± s.d., *n* = 3 replicates; *P* value by two-tailed, two-sample *t* test. **d**, Validation of ectopic MAGOH-V5 expression in ChagoK1 cells (related to Fig. 1f). Cells were transduced with lentivirus encoding V5-tagged MAGOH and western blotting was performed using an anti-MAGOH/B antibody. The experiment was repeated twice with similar results. **e**, Cell viability measured upon *MAGOHB* knockdown in ChagoK1 cells with or without ectopic expression of untagged MAGOH. Data are presented as mean ± s.d., *n* = 6 replicates. Center wells analyzed in each condition; the experiment was repeated using two separate untagged MAGOH overexpression constructs with similar results. **f**, Validation of ectopic untagged MAGOH expression by western blotting in ChagoK1 cells. Results from a single experiment, repeated once in H1437 cells with similar results.

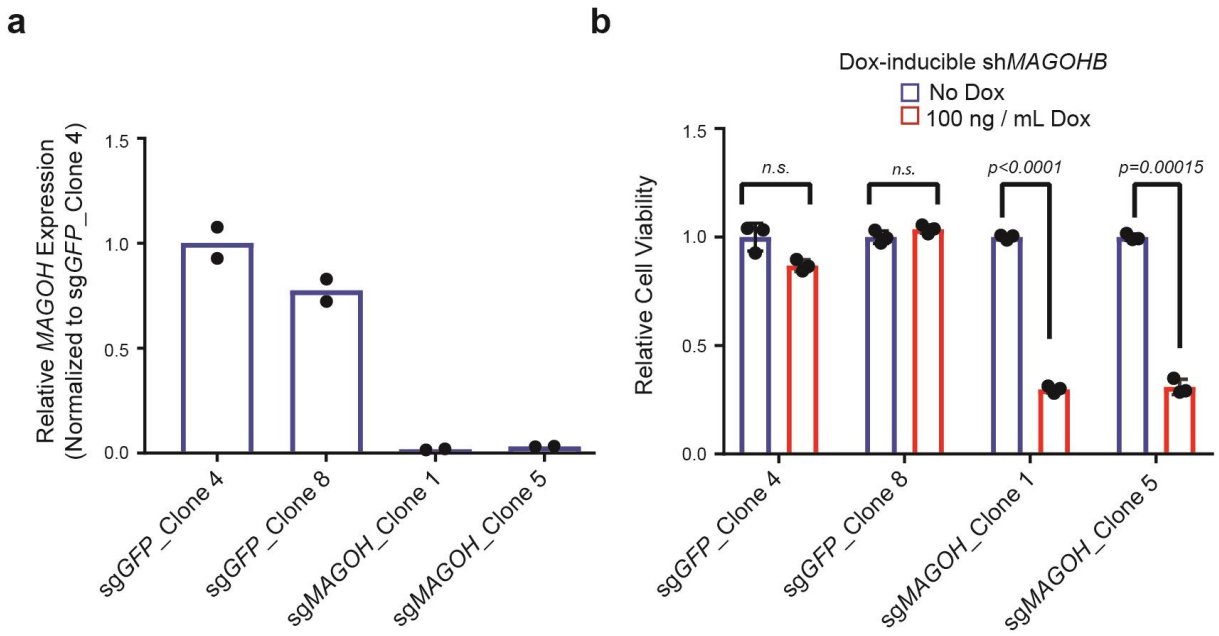

Supplementary Figure 5

Supplementary Figure 5

Knockout of *MAGOH* confers *MAGOHB* dependency.

a, Validation of *MAGOH*-deleted clonal Heya8 cell lines. Heya8 cells, which are copy neutral for *MAGOH*, were transiently transfected with either a control sgRNA (sgGFP) or an sgRNA targeting *MAGOH*. Single-cell clones were derived and *MAGOH* expression was measured by quantitative PCR. Two single-cell clones (sg*MAGOH*_Clone 1 and sg*MAGOH*_Clone 5) demonstrated ablation of *MAGOH* expression as compared with control clones. Data are presented as relative *MAGOH* expression, normalized to expression in sg*GFP*_Clone 4. Points are shown from $n = 2$ technical replicates. **b**, Single-cell Heya8 clones were transduced with lentivirus encoding a doxycycline-inducible shRNA against *MAGOHB*. Cell viability was assessed 7 d after shRNA induction by CellTiterGlo. Data are presented as viability normalized to the –Dox condition for each cell line. Error bars show mean ± s.d., $n = 3$ replicates from a representative experiment repeated twice; *P* value by two-tailed, two-sample *t* test.

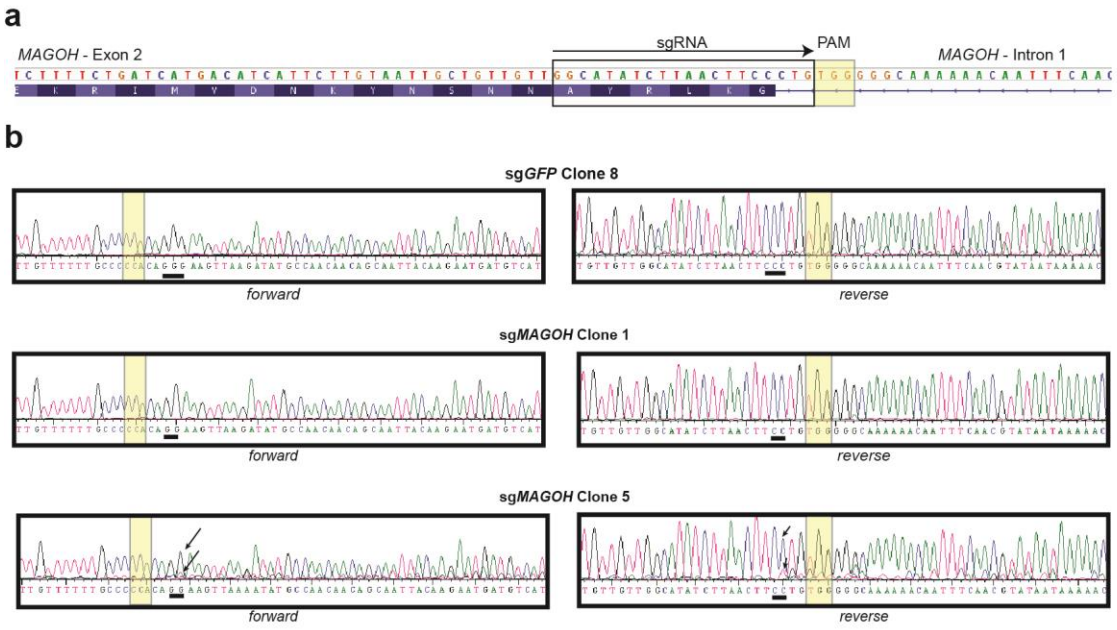

Supplementary Figure 6

Supplementary Figure 6

Validation of sgRNAs used for *MAGOH* knockout in Heya8 cells.

a, Schematic showing the sgRNA target and PAM site, which lies near the intron 1–exon 2 junction of *MAGOH*. **b**, Sanger sequencing traces around the *MAGOH* sgRNA cut site, from single-cell Heya8 clones derived from cells transduced with either non-targeting guide (sg*GFP*) or guide against *MAGOH*. In both *MAGOH*-deleted clones (clones 1 and 5), an indel at the indicated position (black underline) occurs in a similar location and could cause a frameshift. In clone 5, mixed peaks may suggest distinct editing events on each allele. Ablation of *MAGOH* expression in these clones is shown in Supplementary Fig. 5.

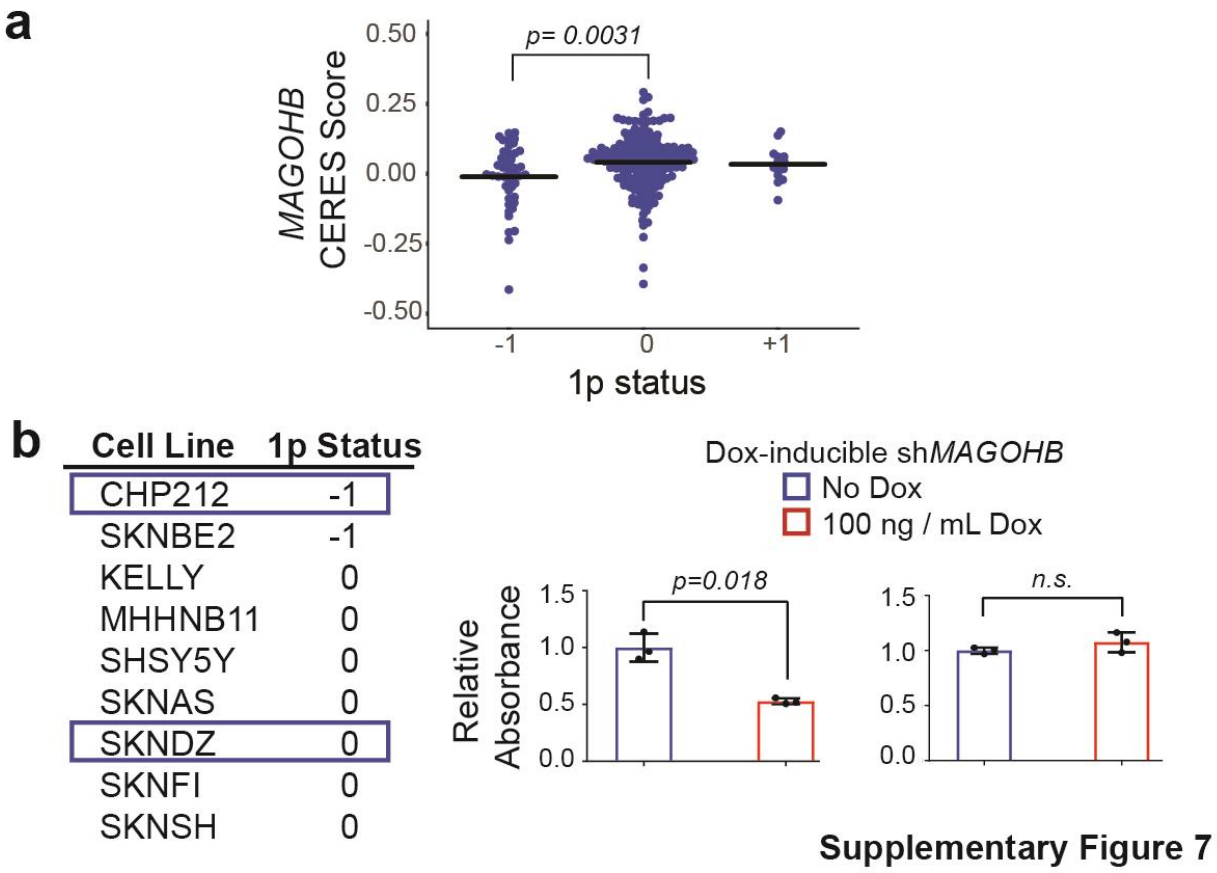

Supplementary Figure 7

***MAGOHB* dependency in cells with chromosome 1p loss.**

a, Distribution of *MAGOHB* CERES dependency scores in screened cell lines with chromosome 1p loss (–1, $n = 46$), 1p neutral status (0, $n = 177$), or 1p gain (+1, $n = 14$). 1p-deleted cell lines are significantly more dependent on *MAGOHB* than are 1p neutral cell lines; *P* value calculated by two-sample, one-sided Welch's *t* test. Horizontal lines indicate means. **b**, Validation of selective *MAGOHB* dependency in 1p-deleted neuroblastoma cells. CHP212 (1p-deleted, left) or SKNDZ (1p-neutral, right) neuroblastoma cells were transduced with lentivirus expressing a doxycycline-inducible shRNA against *MAGOHB* and seeded for colony formation assay in either the absence of doxycycline or the presence of 100 ng/ml doxycycline. Colony formation was quantified by destaining of crystal violet and measurement of absorbance at 595 nm. Data are presented as mean ± s.d., $n = 3$ replicates; *P* value by two-tailed, two-sample *t* test.

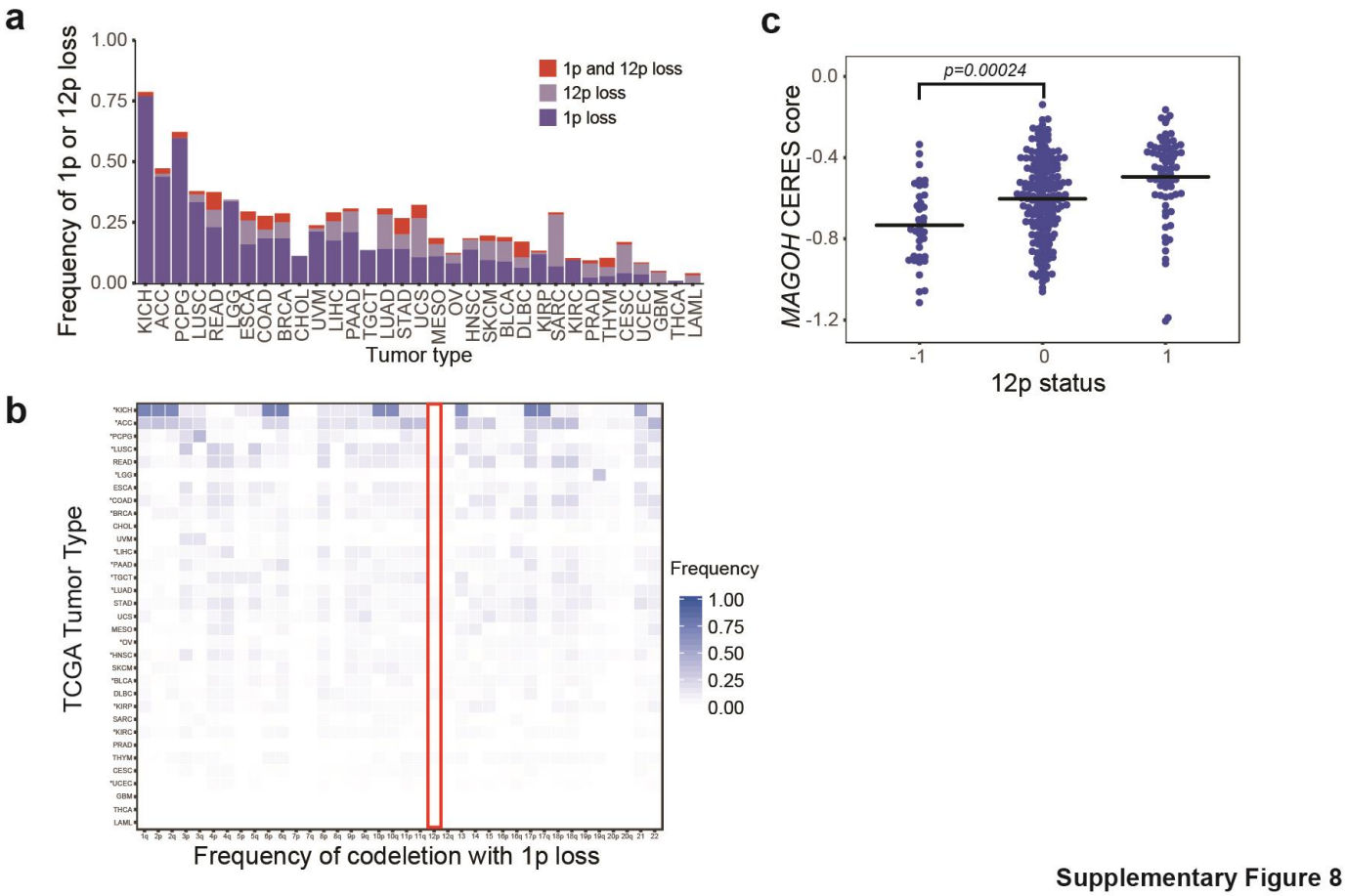

Supplementary Figure 8

Supplementary Figure 8

***MAGOH* dependency in cells with chromosome 12p loss.**

a, Frequency of chromosome 12p and 1p loss across TCGA cohorts. **b**, Heat map of arm-level deletion events co-occurring with chromosome 1p loss across TCGA cohorts. Cohorts in which chromosome 1p co-deletion with chromosome 12p are significantly mutually exclusive (as compared with all possible 1p co-deletion events) are indicated by an asterisk. **P* < 0.05 by one-sided binomial test. Range of TCGA cohort sizes analyzed, *n* = 36 (CHOL) to *n* = 1,030 (BRCA). **c**, Distribution of *MAGOH* CERES dependency scores in screened cell lines with chromosome 12p loss (–1, *n* = 37), 12p neutral status (0, *n* = 169), or 12p gain (1, *n* = 69). 12p-deleted cell lines are significantly more dependent on *MAGOH* than are 12p-neutral cell lines. Horizontal lines indicate means; *P* value by Welch's two-sample one-sided *t* test.

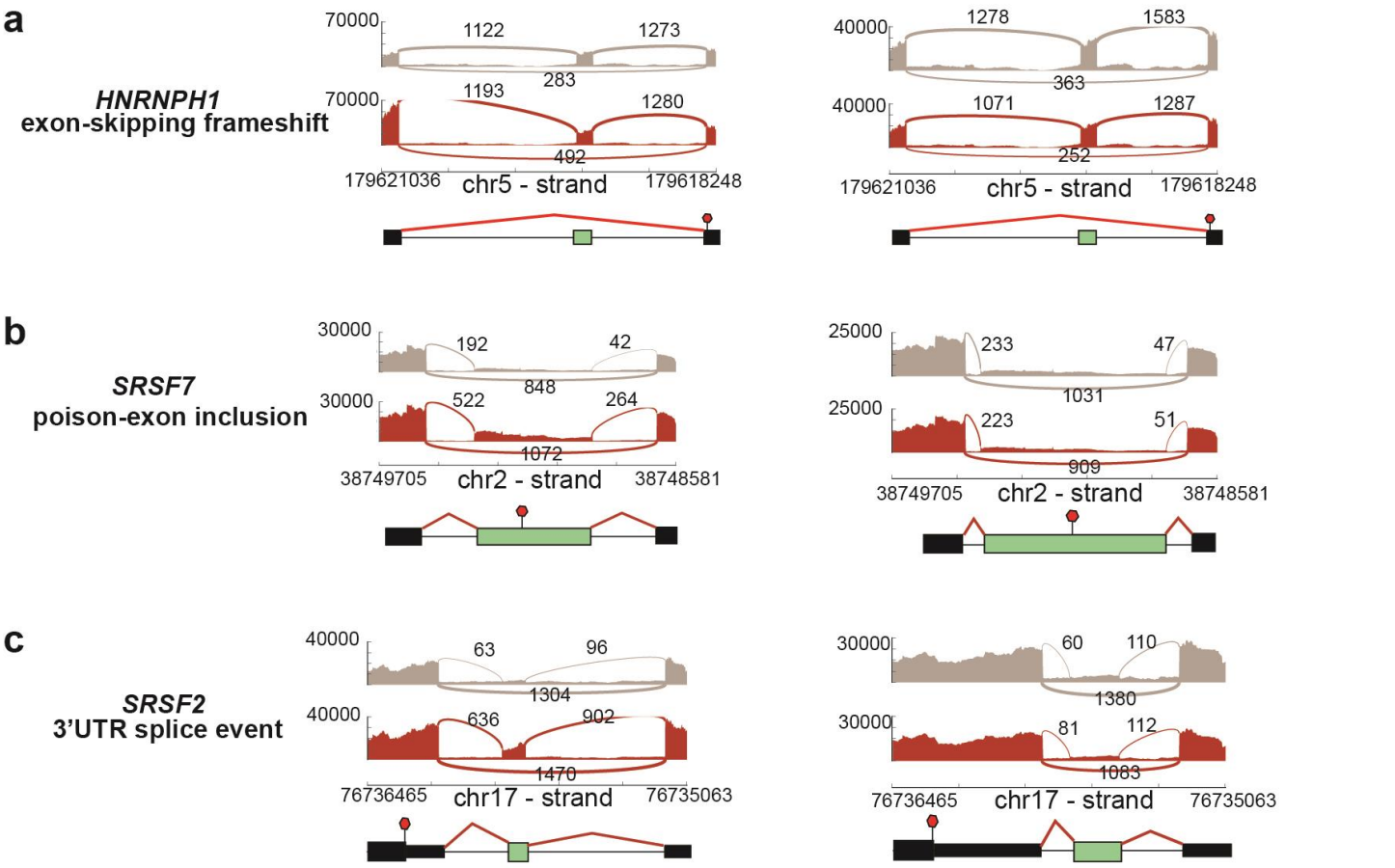

Supplementary Figure 9

Supplementary Figure 9

RNA sequencing reveals multiple splicing events with potential effects on AS-NMD loops upon *MAGOHB* knockdown in ChagoK1 cells, but not MAGOH-V5-reconstituted ChagoK1 cells.
a–**c**, Sashimi plots around ultraconserved elements reported to regulate AS-NMD loops in either the absence (gray) or presence (red) of *MAGOHB* knockdown in ChagoK1 cells (left panels) or MAGOH-V5-reconstituted ChagoK1 cells (right panels) for the genes *HNRNPH1* (**a**), *SRSF7* (**b**), and *SRSF2* (**c**). Schematics depict splice-site usage events that result in the creation of premature termination codons. Numbers of junction-spanning reads averaged over three replicates for each condition are as indicated.

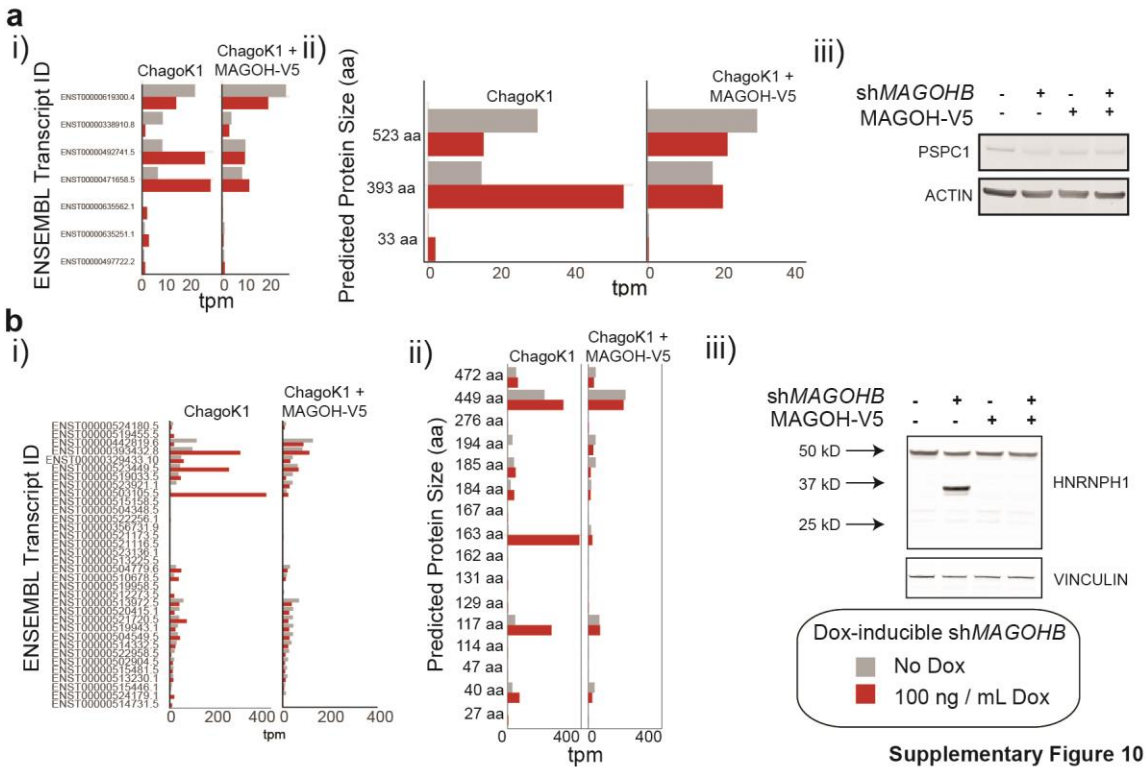

Supplementary Figure 10

Supplementary Figure 10

Alterations in splice isoform usage upon *MAGOHB* knockdown in a *MAGOH*-deleted context and predicted changes in protein levels of affected genes.

a,**b**, Isoform abundances (i) and predicted expression changes on the protein level (ii) for the genes *PSPC1* (**a**) and *HNRNPH1* (**b**) in ChagoK1 cells and MAGOH-reconstituted ChagoK1 cells with (red) or without (gray) *MAGOHB* knockdown. To predict effects on protein expression, isoforms were grouped by predicted protein-coding size as described in the Methods. Protein expression levels were assessed by western blotting (iii). **a (**iii), Western blotting for PSPC1 shows a dominant band presumed to correspond to the 523-aa/58-kDa predicted protein isoform. Western blots are from a representative experiment repeated twice. **b** (iii), Western blotting for HNRNPH1 shows a dominant truncated isoform for HNRNPH1 (~35 kDa) observed upon *MAGOHB* knockdown in a *MAGOH*-deleted context that does not exactly correspond in size to what is expected based on RNA-sequencing data; this truncated species has not been fully characterized. Western blots are from a representative experiment repeated three times.

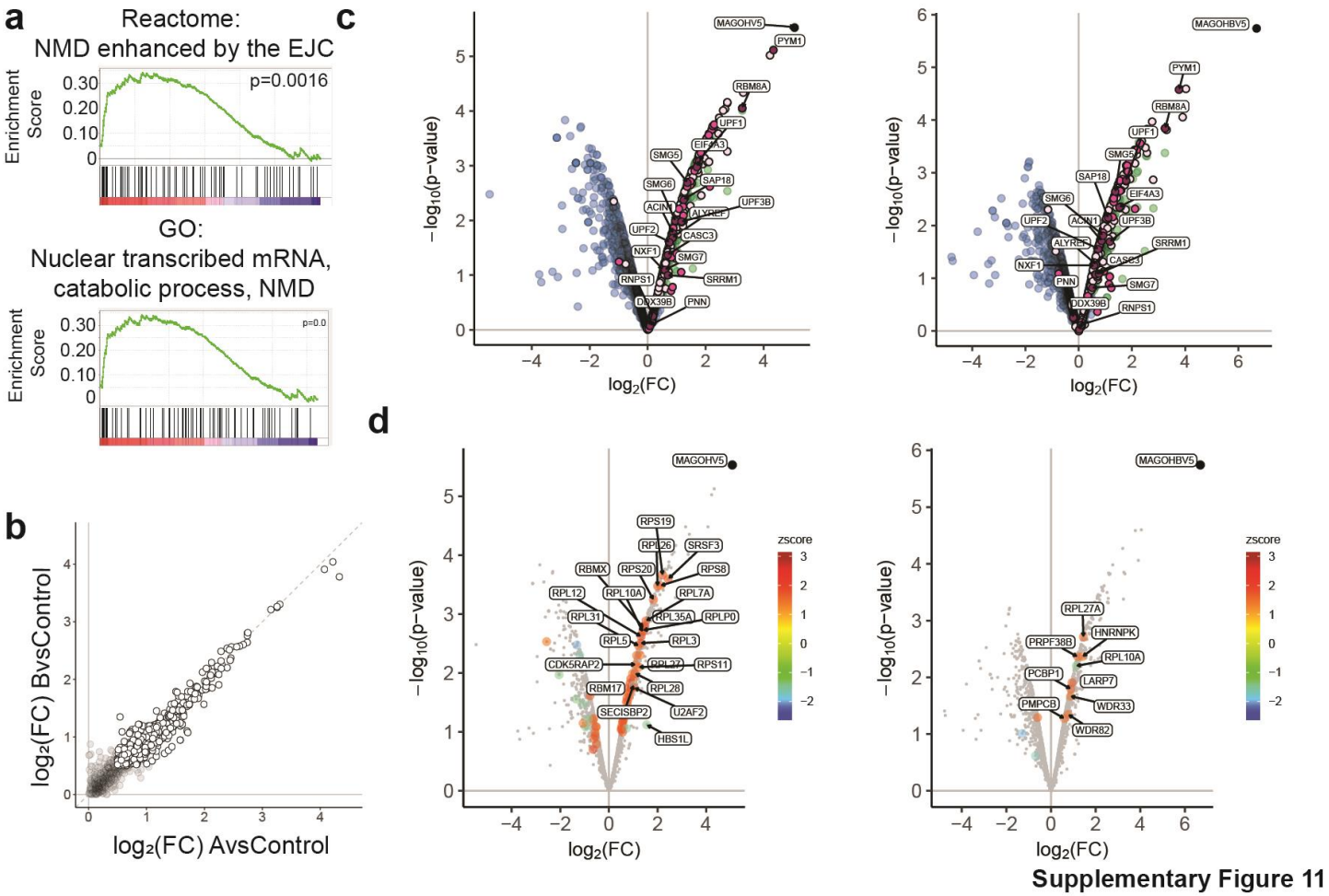

Supplementary Figure 11

Supplementary Figure 11

***MAGOH* and *MAGOHB* dependencies are correlated with dependencies on other members of the MAGOH/MAGOHB interactomes.**

a, Gene set enrichment analysis reveals enrichment of nonsense-mediated decay/exon junction complex gene sets among gene dependencies (n = 6,304) correlated with *MAGOH* copy number. Significance was assessed by running preranked GSEA using the gene dependency list as described (Methods). **b**, Immunoprecipitation–mass spectrometry was performed on MAGOH-V5- or MAGOHB-V5-expressing 293T or parental 293T cells ('control') using an anti-V5 antibody. Fold enrichment of interacting proteins over control for MAGOH-V5 (x axis) or MAGOHB-V5 (y axis) IPs is shown. Open circles indicate interactors with $\log_2$ (fold change) enrichment > 0.5 over control. Baits are not shown on the plot. **c**, Volcano plot for MAGOH-V5- (left) or MAGOHB-V5- (right) interacting proteins. The color scale depicts proteins in the following classes (from light pink to maroon): RNA binding, S ribosomal, EJC/NMD pathway member. Labeled proteins highlight selected EJC/NMD members found in the IPs. Significance was determined by moderated t test to calculate P values for the n = 1,995 genes from the IP, corrected for multiple hypotheses (FDR). **d**, MAGOH-V5 (left) or MAGOHB-V5 (right) interactomes overlaid with gene dependencies correlated with *MAGOH* (left) or *MAGOHB* (right) dependency. Dependency–dependency correlations with z scores >1.5 or <–1.5 are colored according to the scale. Gene dependencies correlated to *MAGOH* dependency (z > 1.5) are enriched among MAGOH-V5 interactors ($\log_2$ FC > 0.7) ($P = 1.5 \times 10^{-4}$) and gene dependencies correlated to *MAGOHB* dependency (z > 1.5) are enriched among MAGOHB-V5 interactors ($\log_2$ FC > 0.7) (P = 0.051). P values were calculated by one-sided Fisher exact test on the population of n = 380 genes (the overlap set of IP genes with $\log_2$ FC > 0.7 and the dependency data). Labels indicate proteins with z > 1.5 and $\log_2$ FC > 1 for the MAGOH-V5 plot and z > 1.5 and $\log_2$ FC > 0.5 for the MAGOHB-V5 plot.

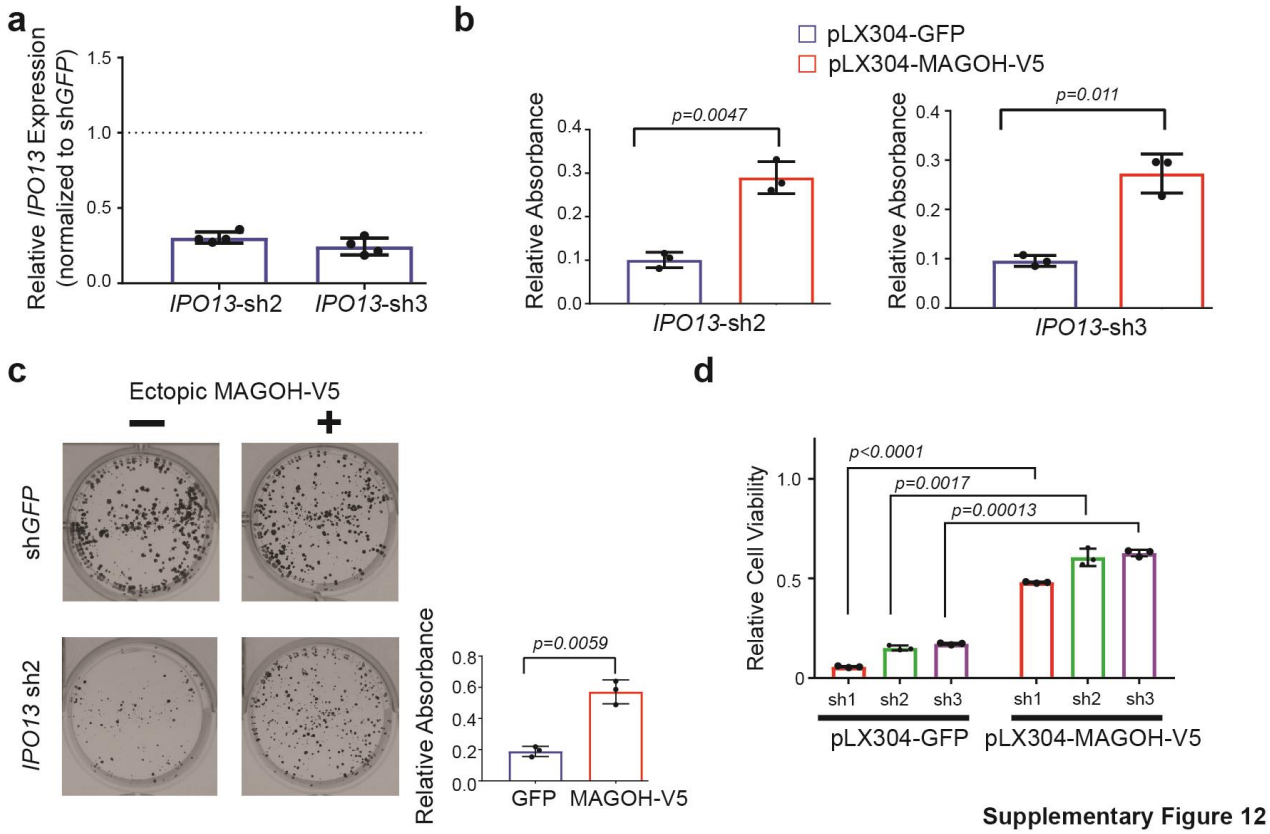

Supplementary Figure 12

Supplementary Figure 12

Additional validation of *IPO13* dependency in *MAGOH*-deleted cells.

a, *IPO13* knockdown was verified in H460 cells by quantitative PCR. H460 cells were transduced with lentivirus expressing either control shRNA (sh*GFP*) or shRNAs against *IPO13* in the pLKO.1 vector. *IPO13* expression levels were assessed 72 h after selection using quantitative PCR. Expression levels are shown as normalized to control (sh*GFP*) condition. Data are presented as mean ± s.d., $n = 4$ technical replicates. **b**, Quantification of the colony formation assay (related to Fig. 3d). Following crystal violet staining, wells were destained and measurement of absorbance at 595 nm was performed for quantification of colony number; data are normalized to absorbance in the sh*GFP* condition. Data are presented as mean ± s.d., $n = 3$ replicates; *P* value by two-tailed two-sample *t* test. **c**, Clonogenic capacity was measured in *MAGOH*-deleted H1437 cells upon *IPO13* knockdown in either the absence (left) or presence (right) of MAGOH-V5 reconstitution. Destaining and measurement of absorbance at 595 nm was performed for quantification of colonies formed; data are normalized to absorbance in the sh*GFP* condition. Data are presented as mean ± s.d., $n = 3$ replicates; *P* value by two-tailed two-sample *t* test. **d**, Cell viability was measured in *MAGOH*-deleted H1437 cells upon *IPO13* knockdown in either the absence (left) or presence (right) of MAGOH-V5 reconstitution. Data represent relative cell viability normalized to the sh*GFP* condition. Data are presented as mean ± s.d., $n = 3$ replicates; *P* value by two-tailed two-sample *t* test.

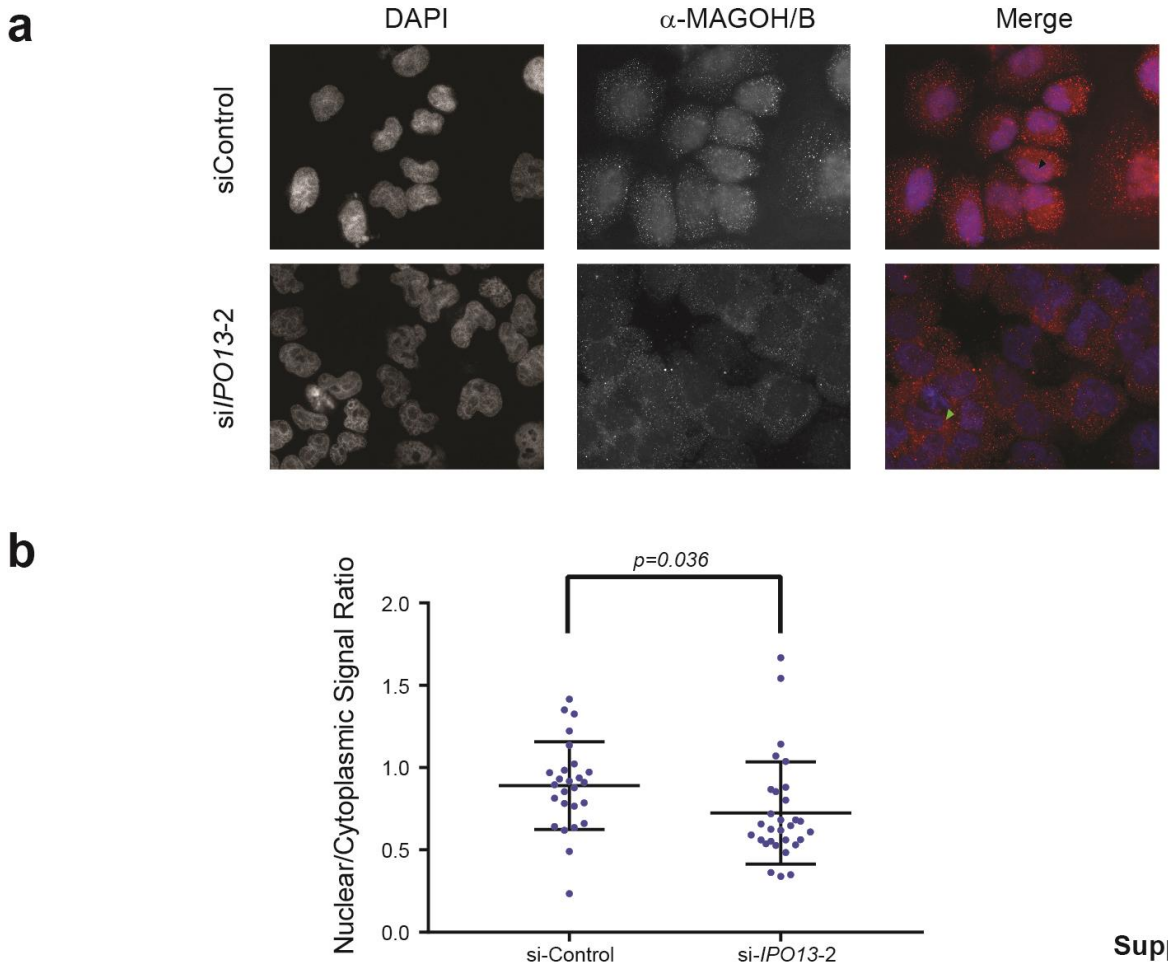

Supplementary Figure 13

***IPO13* knockdown in the setting of *MAGOH* deletion disrupts normal MAGOH/B localization and may interfere with EJC shuttling.**

a, Representative fields of immunofluoresence staining of MAGOH/B in H460 cells in either the absence (top) or presence (bottom) of siRNA-mediated *IPO13* knockdown. *IPO13* knockdown in the setting of *MAGOH* deletion leads to decreased nuclear (black arrowhead) signal in favor of cytoplasmic (green arrowhead) signal. **b**, Quantification of fluorescence signal (nuclear/cytoplasmic ratio) in H460 cells transfected with either control siRNA or si-*IPO13*-2. Quantification was performed on three random fields per condition (n = 26 cells for control; n = 30 cells for si-*IPO13*-2) by ImageJ. Data are presented as mean ± s.d.; P value by two-tailed two-sample t test.

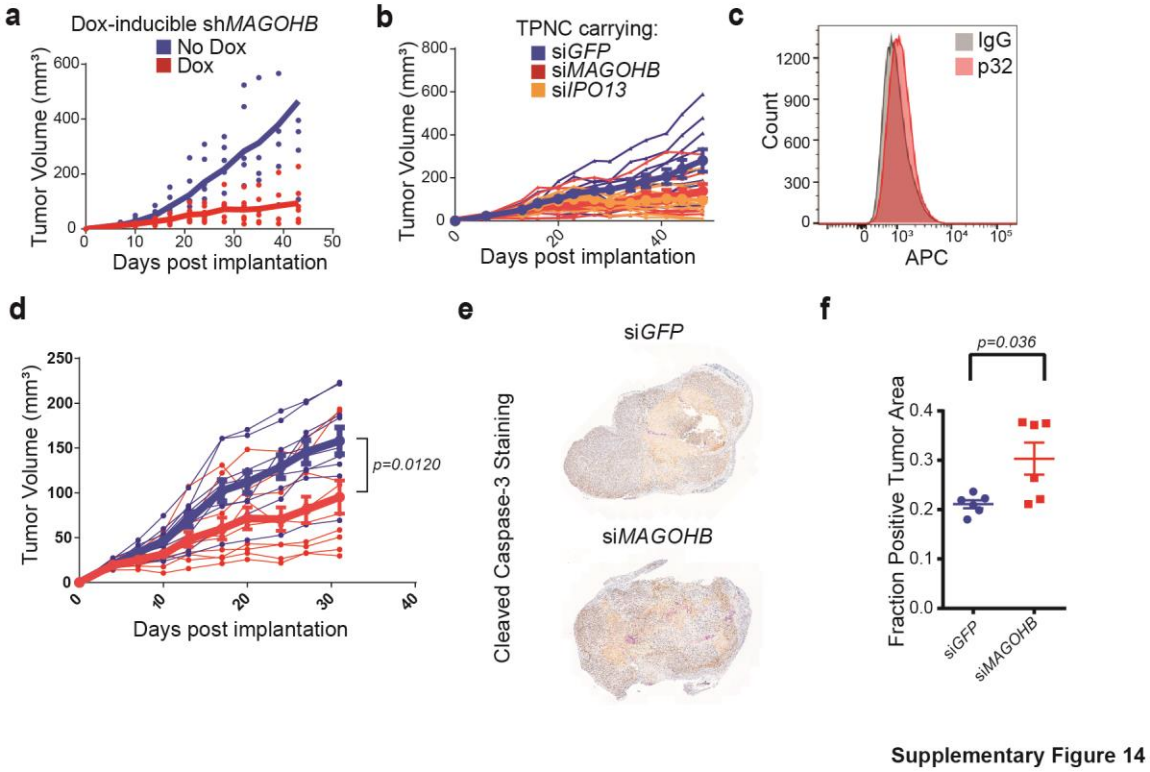

Supplementary Figure 14

Supplementary Figure 14

H1437 xenografts can be targeted by TPNCs carrying siRNA against *MAGOHB* or *IPO13*.
a, Individual tumor volumes for the xenograft experiment shown in Fig. 4b (*n* = 6 tumors per condition). The solid line connects the mean tumor volume at each time point. **b**, Individual tumor volumes for the xenograft experiment shown in Fig. 4e (*n* = 10 tumors per condition). Solid line overlays show mean ± s.e.m. for each condition at each time point. **c**, Surface expression for p32 (receptor for LyP-1-containing nanocomplexes) in H1437 cells, as assessed by flow cytometry. Results are from single experiment. **d**, H1437 tumor xenograft experiment performed by intra-tumoral injection of LyP-1-containing nanocompexes carrying either si*GFP* or si*MAGOHB* cargo. Thin lines show tumor growth in individual mice (*n* = 10 tumors per group). Solid lines show mean ± s.e.m. for each condition. **e**, Representative staining for cleaved caspase-3 in an si*GFP*-treated mouse (top) and an si*MAGOHB*-treated mouse (bottom) using LyP-1-based tumor-penetrating nanocomplexes. Staining was performed on *n* = 6 tumors per group (randomly selected). **f**, Quantification of staining levels in six randomly selected tumors from each group. Data are presented as mean ± s.d.; *P* value by two-tailed, two-sample *t* test.

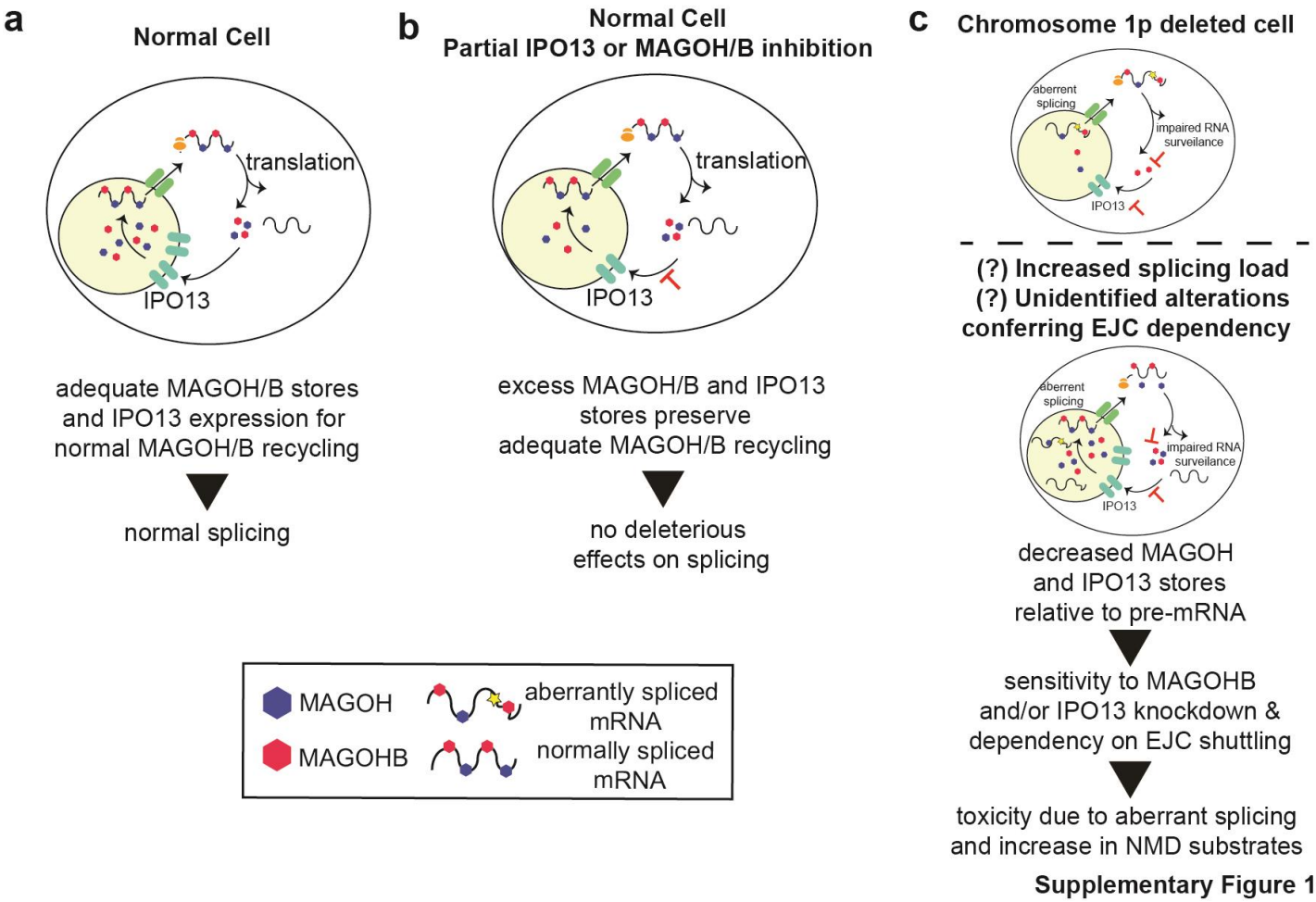

Supplementary Figure 15

A model for *MAGOH*/*B* and *IPO13* dependency.
a,**b**, Cells without alterations in *MAGOH*/*B* and *IPO13* have adequate MAGOH/B and IPO13 to tolerate partial inhibition of any of these factors. **c**, However, hemizygous loss of *MAGOH* and/or *IPO13*, as occurs in chromosome 1p loss, can sensitize cells to *MAGOHB* or *IPO13* inhibition (top panel). An increased dependency on EJC function/shuttling may also occur in other states perhaps driven by an increased need for splicing or by somatic alterations in as-yet-unknown factors (bottom panel).

Supplementary Note

This supplementary note contains additional explanatory text that could not be included in the main manuscript due to space constraints, as well as explanatory captions for selected supplementary tables.

ADDITIONAL BACKGROUND ON PARALOG DEPENDENCIES

The notion of paralog dependencies was first set forth over two decades ago[1] and subsequent functional genomic approaches have confirmed that the inactivation of certain tumor suppressor genes can confer dependency on functionally redundant paralogs, in some cases due to the co-deletion of nearby passenger genes (i.e. *ARID1B* as a dependency in *ARID1A*-mutant cancers[2], *SMARCA2* as a dependency in a *SMARCA4*-mutant cancers[3], *CDH3* as a dependency in *CDH1*-deleted cancers[4], *ME3* as a dependency in cancers with deletion of the *ME2* gene neighboring the *SMAD4* gene[5], or *ENO2* as a dependency in glioblastomas with homozygous deletion of *ENO1*[6]).

ANALYSIS OF PARALOG DEPENDENCIES IN GENOME-SCALE shRNA and CRISPR SCREENS

Paralogs were defined as gene pairs sharing >25% sequence identity at the DNA level; at this identity threshold, we observed more frequent co-expression of paralogs, thus yielding the potential for mutual interdependence and genetic vulnerability **(Supplementary Figure 1)**. Based on this definition, database query yielded 56,797 "test pairs" ($paralog_1$,$paralog_2$) in which dependency on $paralog_1$ could be tested in the setting of loss of $paralog_2$. Of these, in the shRNA screening data, there were 10,287 test pairs in which $paralog_1$ was a 2σ differential dependency (**Online Methods**). Among these were 3,940 test pairs (1970 "gene pairs") in which both $paralog_1$ and $paralog_2$ were in the 2σ differential dependency set. Thus, these pairs could be tested for symmetry ($paralog_1$ dependency with $paralog_2$ loss and $paralog_2$ dependency with $paralog_1$ loss). This analysis revealed 14 significant symmetric paralog dependencies (7 pairs) and 153 significant asymmetric paralog dependencies at $q < 0.05$. In the CRISPR dataset, there were 8973 test pairs subjected to differential dependency testing. Of these, 3186 test pairs (1593 gene pairs) were testable for symmetry. This revealed 14 significant symmetric paralog dependencies (7 pairs) and 111 significant asymmetric paralog dependencies at $q < 0.05$. In both cases, paralog loss of function was defined as one or more of the following: copy number loss, low RNA expression, low protein expression, hypermethylation, or damaging mutation.

ANALYSIS OF DEPENDENCIES IN *MAGOH*-DELETED CELLS

To identify gene dependencies correlated with hemizygous *MAGOH* deletion, we analyzed the genome-wide shRNA screening data described[7] for all genes showing differential dependency across the cell lines screened[7]. This differential dependency set consists of 6,305 genes (**Online Methods**). As *MAGOH* inactivation was most frequently a result of copy number loss of the gene, we focused on this mode of *MAGOH* inactivation for this analysis. Of 445 cell lines analyzed for both *MAGOH* absolute copy number status and gene dependency, there were 83 cell lines with hemizygous *MAGOH* deletion (19%) and 362 (81%) without *MAGOH* deletion. *MAGOHB* was by far the top differential gene dependency in cells with deletion of *MAGOH* (**Fig. 1c, Supplementary Tables 4-5**).

ALTERED ISOFORM DISTRIBUTIONS OF SPLICING FACTORS IN THE CONTEXT OF MAGOH/B INSUFFICIENCY

We observed that *MAGOHB* knockdown in ChagoK1 cells upregulates an NMD isoform of the *HNRNPDL* gene by activating an exon within the 3'-UTR of the gene. As this transcript fails to be degraded by NMD in the setting of insufficient MAGOH/B, it can be translated into protein, thus potentially disrupting a negative feedback, autoregulatory AS-NMD circuit and converting it into a feed-forward loop that leads to increased HNRNPDL expression (**Fig. 2e**). Perturbations in RNA isoform distributions of multiple other splicing-related genes were also observed upon *MAGOHB* knockdown in ChagoK1 cells, but not in MAGOH-reconstituted ChagoK1 cells and in some cases effects were seen on the protein level (**Supplementary Figures 9-10**). However, we note that the net impact of such RNA isoform perturbations on functional protein levels in affected genes is complex and the two may not always perfectly correspond. Multiple factors may influence ultimate protein levels, including: 1) the total abundance of isoforms coding for functional protein; 2) the activity of the NMD pathway on potential NMD substrates; 3) the translational efficiency of those transcripts (the latter of which may be impacted by splice events affecting the 3' UTR length[8]); and 4) the stability of translated protein products.

MASS SPECTROMETRY OF MAGOH AND MAGOHB COMPLEXES

We performed gene-set enrichment analysis on the list of gene dependencies correlated with *MAGOH* deletion and indeed observed a significant enrichment for exon-junction complex-related genes among these dependencies (**Supplementary Figure 11**). Mass spectrometry of MAGOH- and MAGOHB-associated complexes also revealed that the MAGOH- and MAGOHB-interactomes were significantly enriched for gene dependencies correlated to *MAGOH* and *MAGOHB* dependency in our genome-wide shRNA screening data, suggesting a dependency network supported by complementary biochemical and genetic approaches (**Supplementary Figure 11; Supplementary Tables 9-11**). Nonetheless, these correlated dependencies were significantly weaker than reciprocal *MAGOH/B* and *IPO13* dependencies. We conclude that, while *MAGOH/B* deletion may unmask a broader dependency on splicing-related genes or pathways, the dominant vulnerabilities in these contexts remain the redundant essentiality of *MAGOH/B*.

IPO13 DEPENDENCY IN MAGOH OR MAGOHB-DEPENDENT CELLS

Of 243 cell lines assayed for *IPO13* dependency by shRNA, we observed 33 lines that were strongly dependent on *IPO13* (DEMETER score < -2). Of these, 18/33 were also dependent on either *MAGOH*, *MAGOHB*, or both (*MAGOH, MAGOHB*, or both DEMETER scores < -2). Of the remaining 210 cell lines less dependent on *IPO13* (DEMETER score > -2), only 22/210 were dependent on either *MAGOH*, *MAGOHB*, or both. This suggests that *IPO13* dependency and *MAGOH/B* dependency frequently co-occur ($p<0.0001$ by two-tailed Fisher's exact test).

ADDITIONAL EXPLANATORY CAPTIONS FOR SELECTED SUPPLEMENTARY TABLES

Supplementary Table 1. Analysis of reciprocal paralog dependencies in genome-scale shRNA screening data.

Significant paralog dependencies were determined from a starting set of 10,287 paralog pairs. Details as described in main text and Online Methods. Column header definitions are as follows.

Dep_Gene: Gene for which the DEMETER Gene Scores are tested between groups

Loss_Gene: Status of this paralog of the Dep_Gene is used to define the two groups for comparison (loss vs. wild-type). “Loss” defined based on copy number loss, low protein/RNA expression, hypermethylation, or damaging mutation).
EffectSize: Difference in mean DEMETER score for the Dep_Gene between cell lines that have loss of the paralog gene and those that are wild-type
t_stat: Moderated t-statistic for the two class comparison calculated using Limma
log_odds: Log-odds that there is differential dependency on the Dep_Gene
min_samples: Number of cell lines that have DEMETER scores for the Dep_Gene as well as RNAseq expression data and damaging mutation calls for the Loss_Gene
p.left: Raw p-value for two class comparison calculated using Limma
qvalue: Benjamini & Hochberg correction for multiple hypothesis testing
symmetric: Both grouping by the Loss_Gene and comparing the DEMETER scores of the Dep_Gene as well as grouping by the Dep_Gene and comparing the DEMETER scores of the Loss_Gene have an FDR < 5%
paralog_evaluable: Indicates whether the reverse comparison of Dep_Gene and Loss_Gene was able to be tested in the analysis (some genes are not classified as lost in any of the cell lines or may not have DEMETER profiles indicating any strong dependencies)
Total_samples: Number of cell lines that have DEMETER scores for the Dep_Gene
SixSigma_Count: Number of cell lines that have at least a 6sigma outlier dependency on the Dep_Gene

Supplementary Table 2. Analysis of reciprocal paralog dependencies in genome-scale CRISPR/Cas9 screening data.

Significant paralog dependencies were determined from a starting set of 8973 paralog pairs (CRISPR). Details as described in main text and Online Methods. Column header definitions are as in caption to Supplementary Table 1.

Supplementary Table 3. Gene ontology enrichment among genes found to be symmetric or asymmetric paralog dependencies in analysis of shRNA and CRISPR screening data.

Union of symmetric or asymmetric paralog dependencies from both CRISPR and shRNA screens was used in ontology analysis.

Supplementary Table 5. Results of PARIS analysis to identify gene dependencies correlated with *MAGOH* deletion across CCLE cell lines.

Dependencies are ranked in descending order of RNMI significance statistic.

Supplementary Table 12. Gene Dependencies correlated to *MAGOH* and *MAGOHB* dependency.

Z-scored correlation between *MAGOH* or *MAGOHB* dependency and dependency on other assayed genes is listed.

SUPPLEMENTARY NOTE REFERENCES

1. Frei, E. Gene deletion: a new target for cancer chemotherapy. *The Lancet* **342,** 662–664 (1993).
2. Helming, K. C. *et al.* ARID1B is a specific vulnerability in ARID1A-mutant cancers. *Nat. Med.* **20,** 251–254 (2014).
3. Hoffman, G. R. *et al.* Functional epigenetics approach identifies BRM/SMARCA2 as a critical synthetic lethal target in BRG1-deficient cancers. *Proc. Natl. Acad. Sci.* **111,** 3128–3133 (2014).
4. D'Antonio, M. *et al.* Recessive cancer genes engage in negative genetic interactions with their functional paralogs. *Cell Rep.* **5,** 1519–1526 (2013).
5. Dey, P. *et al.* Genomic deletion of malic enzyme 2 confers collateral lethality in pancreatic cancer. *Nature* **542,** 119–123 (2017).
6. Muller, F. L. *et al.* Passenger deletions generate therapeutic vulnerabilities in cancer. *Nature* **488,** 337–342 (2012).
7. Tsherniak, A. *et al.* Defining a Cancer Dependency Map. *Cell* **170,** 564-576.e16 (2017).
8. Shi, J., Pabon, K. & Scotto, K. W. Methylxanthines Increase Expression of the Splicing Factor SRSF2 by Regulating Multiple Post-transcriptional Mechanisms. *J. Biol. Chem.* **290,** 14986–15003 (2015).